

High resolution charge-exchange spectroscopic measurements of aluminum impurity ions in a high temperature plasma

This article has been downloaded from IOPscience. Please scroll down to see the full text article.

2012 Plasma Phys. Control. Fusion 54 012002

(<http://iopscience.iop.org/0741-3335/54/1/012002>)

View [the table of contents for this issue](#), or go to the [journal homepage](#) for more

Download details:

IP Address: 128.104.166.215

The article was downloaded on 16/12/2011 at 20:34

Please note that [terms and conditions apply](#).

BRIEF COMMUNICATION

High resolution charge-exchange spectroscopic measurements of aluminum impurity ions in a high temperature plasma

S T A Kumar^{1,2}, D J Den Hartog^{1,2}, B E Chapman¹, M O'Mullane³,
M Nornberg^{1,2}, D Craig⁴, S Eilerman¹, G Fiksel⁵, E Parke¹ and J Reusch¹

¹ Department of Physics, University of Wisconsin-Madison, Madison, WI, USA

² Center for Magnetic Self-Organization in Laboratory and Astrophysical Plasmas,
University of Wisconsin-Madison, Madison, WI 53706, USA

³ Department of Physics, University of Strathclyde, Glasgow, G4 ONG, UK

⁴ Wheaton College, Wheaton, IL, USA

⁵ Laboratory for Laser Energetics, University of Rochester, NY, USA

E-mail: stkumar@wisc.edu

Received 11 July 2011, in final form 14 November 2011

Published 15 December 2011

Online at stacks.iop.org/PPCF/54/012002

Abstract

Charge-exchange recombination spectroscopy, which is generally used to measure low- Z impurities in fusion devices, has been used for measuring Al^{+11} and Al^{+13} impurities in the Madison Symmetric Torus reversed field pinch. To obtain the impurity ion temperature, the experimental emission spectrum is fitted with a model which includes fine structure in the atomic transition. Densities of these two ionization states, calculated from charge-exchange emission brightness, are used in combination with a collisional radiative model to estimate the abundance of all other charge states of aluminum in the plasma and the contribution of aluminum to the effective ionic charge of the plasma.

(Some figures may appear in colour only in the online journal)

Charge-exchange recombination spectroscopy (CHERS) has been widely used in high temperature fusion plasmas to measure impurity ion dynamics [1, 2]. Even though this technique was demonstrated to be feasible for medium- Z impurities in the past [3–5], its general use has so far been limited to low- Z impurities like boron, carbon and oxygen, mainly due to the convenience of low- Z ion measurements in obtaining ion temperature and rotation velocity.

High resolution measurements of medium- Z impurities are of great importance both in magnetic and inertial confinement fusion experiments. Medium- Z metallic impurities including aluminum, injected into the plasma via laser blowoff, are often used for impurity transport studies in tokamaks [6]. These measurements, however, are usually

limited to lower charge states, and they are often chord-averaged. Medium- Z gaseous impurities have also been studied in tokamaks using soft-x-ray emission measurements [7]. In inertial confinement fusion experiments, spectroscopic measurements of tracer aluminum impurity ions at higher charge states are used to diagnose properties of the dynamic hohlraum [8]. Spatially localized and temporally resolved measurements of medium- Z impurities, along with those of standard low- Z impurities, could also greatly help in validating existing impurity transport models for fusion devices.

In this paper, we present high resolution CHERS measurements of fully stripped and helium-like aluminum ions in the Madison Symmetric Torus (MST), a high temperature fusion plasma device utilizing an aluminum plasma facing

wall. Necessary atomic physics data and computer codes are obtained from the Atomic Data and Analysis Structure (ADAS) [9]. Densities of these two ions are then used in a collisional radiative model (without transport) to obtain the abundance of other charge states in the plasma and the contribution of aluminum to the effective ionic charge.

MST is a large, moderate current (≤ 600 kA) reversed field pinch with major radius $R = 1.5$ m, and minor radius $a = 0.52$ m [10]. The plasma facing wall of MST is comprised of 5 cm thick aluminum, which serves both as a vacuum vessel and a single turn toroidal magnetic field coil. Inside the vacuum vessel are tiles and limiters made of graphite, boron nitride and ceramic, which interact with the plasma during a discharge and become a source of impurities. The identified dominant impurities in MST plasmas are aluminum, carbon, oxygen, boron and nitrogen. Ionization balance of these impurities in the plasma depends mainly on the electron temperature (ionization) and the hydrogen neutral density (charge-exchange loss), which are significantly different in various plasma regimes in MST. This paper compliments recent measurements of carbon and boron [11] with the first measurements of aluminum impurity in MST.

Experiments are conducted in deuterium improved confinement plasmas of toroidal plasma current ~ 500 – 550 kA, line-averaged central electron density $n_e \sim (0.8$ – $1) \times 10^{19} \text{ m}^{-3}$, core electron temperature $T_e \sim 1$ – 2 keV and core ion (C^{+6}) temperature $T_i \sim 1$ – 1.5 keV. Improved confinement discharges are achieved via the suppression of magnetic fluctuations using a technique called ‘pulsed parallel current drive’ (PPCD) [12–15]. High electron temperature in these discharges ensures that all low- Z impurities are fully ionized over most of the plasma volume and that higher charge states of aluminum are sufficiently abundant to be spectroscopically measurable.

Distinct features of CHERS on MST, which is primarily used for C^{+6} measurements, are good spatial (~ 2 cm) and temporal (up to $10 \mu\text{s}$) resolution [16–18]. The signal-to-noise is significantly enhanced by differencing signals from two lines-of-sight on poloidal planes that are toroidally separated by ~ 4 cm, to measure simultaneously both on-beam and background (off-beam) emission. Measurements are made at one radial location, for one impurity species, per discharge. However, due to high reproducibility, compilation of results from various similar discharges in MST is possible. The custom-built duo spectrometer [17] used for the measurements has been calibrated for radiant sensitivity, using a tungsten-halogen lamp which is pre-calibrated in the range $\lambda = 300$ to 1100 nm, for absolute impurity density calculations from charge-exchange emission brightness. The charge-exchange and the electron-impact excitation/de-excitation emissions are modeled accurately using fine structure in corresponding atomic transitions, obtained from ADAS, to extract Doppler-broadened emission parameters. The model is necessary for the accurate estimation of the ion temperature when the wavelength span of the fine structure manifold is comparable to or more than the Doppler broadening, which is the case presented in this paper. Details of the model are given elsewhere [18].

Table 1. Effective emission rate coefficient for aluminum and carbon ions, calculated using ADAS, for typical high current MST PPCD discharge parameters: $T_e/T_i = 1.5/1.2$ keV, $Z_{\text{eff}} = 4$, $B_T = 0.5$ T, $n_e = 1 \times 10^{19} \text{ m}^{-3}$, $U_{\text{beam}} = 45$ keV.

Impurity ion	Effective emission rate ($\text{m}^3 \text{ s}^{-1}$)	
	Charge exchange	Electron impact
C VI (343.4 nm)	3.2×10^{-14}	1.6×10^{-19}
Al XI (321.05 nm)	9.9×10^{-14}	3.5×10^{-19}
Al XIII (310.65 nm)	1.3×10^{-13}	1.3×10^{-21}

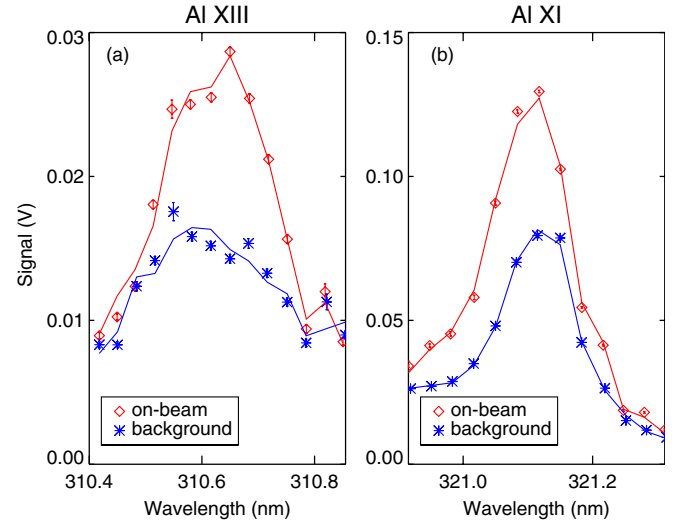


Figure 1. On-beam (charge-exchange + electron-impact) and background (electron-impact) data along with best-fit model results (solid lines) for (a) Al XIII $n = 11$ – 10 transition at $\lambda \sim 310.65$ nm (sh#1110301068) (b) Al XI $n = 10$ – 9 transition at $\lambda \sim 321.05$ nm (sh#1110509028). From calibration, $1 \text{ V} \sim 9 \times 10^8 \text{ photons s}^{-1}$. The ion temperatures obtained from the model are $T_{\text{Al}^{+13}} \sim 1.3$ keV and $T_{\text{Al}^{+11}} \sim 1.1$ keV.

Measurements of aluminum impurity entail the collection of Al XIII and Al XI emissions at $\lambda \sim 310.65$ nm ($n = 11$ to $n = 10$ transition) and ~ 321.05 nm ($n = 10$ to $n = 9$ transition), respectively. These emissions are stimulated by charge exchange between the aluminum ions (Al^{+13} and Al^{+11}) and energetic hydrogen atoms injected radially using a diagnostic neutral beam (nominal parameters: 45–50 keV, 4–5 A, 20 ms pulse length). Data presented in this paper are taken from the central viewing chord ($r/a \sim 0.03$), except for the data shown in figures 2(d) and (e). Attempts to measure Al XII emission were unsuccessful due to spectral contamination by neighbouring line emission. It can be seen from table 1 that for Al XIII emission, the effective rate coefficient for electron-impact excitation is negligible compared with that for charge exchange. Also, the charge-exchange rate coefficient for Al XIII emission is four times higher than that of C VI. This implies that Al^{+13} charge-exchange spectroscopic measurements are possible in fusion devices with a modest amount of injected aluminum impurity.

Local impurity density (n_z) is calculated from the emission brightness using the relation $B_{\text{cx}} = (1/4\pi)n_z\langle\sigma v\rangle \int n_b dl$, where B_{cx} (photons/ $\text{m}^2 \text{ s Sr}$) is the charge-exchange emission brightness (the difference in the area under on-beam and background spectral curves), $\langle\sigma v\rangle$ is the effective emission rate

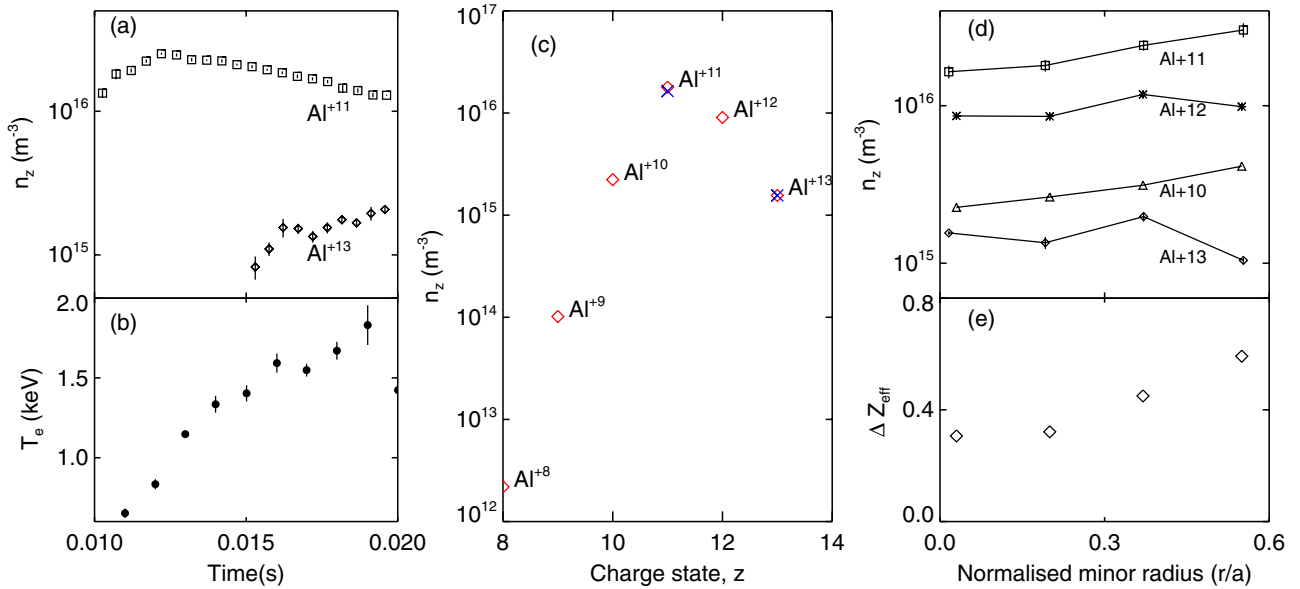


Figure 2. (a) Temporal evolution of Al⁺¹¹ and Al⁺¹³ densities during PPCD (same discharges as in figure 1). (b) Typical temporal evolution of core electron temperature for these discharges. The Al⁺¹³ signal is apparent only when T_e is around 1.5 keV or more. (c) Densities of aluminum charge states (from 8–13) calculated using ADAS collisional radiative model (\diamond) in conjunction with the experimental values (\times). (d) Radial profiles of measured Al⁺¹¹ and Al⁺¹³ densities along with the calculated densities of other higher charge states. (e) Estimated aluminum contribution to the effective ionic charge at various radial locations.

and $\int n_b dl$ is the beam particle density n_b (m⁻³) integrated over the spectrometer line of sight. Effective emission rates are obtained from ADAS. Beam attenuation is modeled using relevant beam stopping reaction cross sections for the three beam-energy components (full, half and one-third energy components are present in the beam with the ratio $E : E/2 : E/3 \sim 60 : 36 : 4\%$), verified with beam-emission and shine-through detector measurements. A 10% uncertainty is estimated in the impurity density, mainly due to uncertainties in the beam attenuation calculations and transmission efficiencies of the viewing lenses.

Figure 1 shows experimental data and the modeling results of on-beam (charge-exchange + electron-impact) and background (electron-impact only) measurements, averaged over ~ 2 ms once the electron temperature rises above 1.5 keV during PPCD. The Al XIII emission is apparent only during this high temperature period in the discharge whereas Al XI shows clear emission throughout PPCD.

The ion temperatures for both ionization states obtained from the model are similar to one another ($T_i \sim 1\text{--}1.5$ keV) and close to the C⁺⁶ temperature measured in similar discharges. This is consistent with the fact that the ion–ion energy equilibration time in these discharges (~ 0.1 ms) is shorter than the global energy confinement time (~ 12 ms) [19]. High ion temperature in these discharges is achieved by trapping the heat produced by magnetic reconnection activity just before the PPCD starting time [19]. Shot-to-shot variation in ion temperature of a few hundred eV is therefore expected due to variation in the initial reconnection heating.

As the fine-structure broadening details are not important for extraction of the total charge-exchange brightness in the impurity density calculations, the difference in the area under on-beam and background spectral curves is used instead of

taking the total brightness from the model. Both methods provide the same results. However, the method of area subtraction is easier, especially when the signal level is too low to be used with the fitting model. Care has been taken to perform this calculation only with higher electron temperatures, when the emission line is prominent. Figure 2(a) shows the temporal evolution of Al⁺¹¹ and Al⁺¹³ densities during PPCD. The initial increase and slow decay of Al⁺¹¹ and the increase of Al⁺¹³ toward the end of the discharge could be explained by the increasing electron temperature (figure 2(b)) throughout PPCD, which modifies the ionization balance of aluminum.

Densities of other aluminum charge states are calculated with the help of a collisional radiative model, ADAS405. This program calculates the fractional abundances of the ions of an element in equilibrium in a thermal⁶ plasma as a function of density and electron temperature [9]. The plasma parameters used for this calculation are $T_e \sim 1.5$ keV, $T_i \sim 1.2$ keV, $n_e \sim 1.2 \times 10^{19}$ m⁻³ and $n_n \sim 7 \times 10^{14}$ m⁻³. The electron temperature (T_e) is measured using a Thomson scattering diagnostic [22]. The neutral deuterium density (n_n), which is varied to match the experimental fractional abundance to that of the model, is very close to the value estimated from D α emission measurements in conjunction with the NENÉ Monte Carlo particle tracing code [23]. The fractional abundance, normalized to the Al⁺¹³ fraction, is multiplied by the experimental value of the Al⁺¹³ density, as shown in figure 2(c). Densities of all charge states of the aluminum impurity (n_z , $z = +1$ to $+13$) are thus obtained. Similar analysis has been performed at other radial locations to obtain

⁶ Effect of runaway electrons in modifying the impurity ionization balance is assumed to be insignificant due to relatively small runaway fraction and high electron temperatures in PPCD [20, 21].

a radial profile of densities of other charge states of aluminum (figure 2(d)) and an estimate of aluminum contribution to the effective ionic charge, $Z_{\text{eff}} = \sum_z n_z z^2 / n_e$ (figure 2(e)).

Both the coronal equilibrium model and experiment show that the Al^{+11} density is higher than that of Al^{+13} , even though the electron temperature is high enough to fully strip most of the aluminum ions in the plasma. This is attributed to the fact that the neutral density in the plasma is relatively high, making the charge-exchange loss of Al^{+13} ions to lower charge states much higher than the ionization rates of Al^{+12} . It has to be noted that this model does not include transport. A more careful analysis including impurity transport is underway.

Measurements of aluminum impurity have considerably helped in improving the understanding of impurity composition and transport in MST. The measurement of aluminum density is motivated partly due to its role in governing transport of light impurities like carbon in MST. For example, our impurity transport model shows that the observed outward convection of low- Z impurities from the core of the plasma [11] could be significantly altered by collisions with medium- Z impurities such as aluminum, if present in large quantities. It has been believed that MST plasmas contain significant level of aluminum impurity as the vacuum vessel is made of aluminum. However, the measured Al^{+11} density is less than that of C^{+6} and O^{+8} by a factor of ~ 5 at the core of the plasma in similar discharges. The estimated aluminum contribution to the Z_{eff} is too small (figure 2(e)) to account for the high Z_{eff} (~ 4 – 6) estimated in the past from x-ray measurements [24]. From measurements of other impurity density profiles and modeling of those measurements, along with the aluminum measurements, it is determined that the radial profile of Z_{eff} is hollow and the core value is less than the x-ray measurements by a factor of ~ 2 – 3 . Preliminary analysis using collisional transport theory shows that this hollow profile could be explained by the temperature screening of impurities due to the ion temperature gradient, but the reason for the discrepancy between the two estimates is not understood at present and will be further studied.

Acknowledgments

This work is supported by the US Department of Energy under cooperative agreement DE-FCO2-05ER54814 for MST and by National Science Foundation -PHY0821899.

References

- [1] Isler R C 1987 *Phys. Scr.* **35** 650
- [2] Fonck R J 1985 *Rev. Sci. Instrum.* **56** 885–90
- [3] Knize R J, Fonck R J, Howell R B, Hulse R A and Jaehnic K P 1988 *Rev. Sci. Instrum.* **59** 1518–20
- [4] Skinner C H, Suckewer S, Cohen S A, Schilling G, Wilson R and Stratton B 1984 *Phys. Rev. Lett.* **53** 458–61
- [5] Whyte D G, Isler R C, Wade M R, Schultz D R, Krstic P S, Hung C C and West W P 1998 *Phys. Plasmas* **5** 3694–9
- [6] Kocsis G, Burger G, Ignacz P N, Kalvin S, Kardon B, Szigeti J, Veres G, Zoletnik S and Bakos J S 1992 *Plasma Phys. Control. Fusion* **34** 1423
- [7] Dux R, Peeters A G, Gude A, Kallenbach A, Neu R and ASDEX Upgrade Team 1999 *Nucl. Fusion* **39** 1509
- [8] Apruzese J P, Clark R W, Davis J, Sanford T W L, Nash T J, Mock R C and Peterson D L 2006 *Rev. Sci. Instrum.* **77** 10F303
- [9] Summers H P 2004 *The Adas User Manual* version 2.6 (www.adas.ac.uk)
- [10] Dexter R N, Kerst D W, Lovell T W, Prager S C and Sprott J C 1991 *Fusion Technol.* **19** 131–9
- [11] Kumar S T A, Den Hartog D J, R M Magee, Fiksel G and Craig D 2011 *Plasma Phys. Control. Fusion* **53** 032001
- [12] Sarff J S, Hokin S A, Ji H, Prager S C and Sovinec C R 1994 *Phys. Rev. Lett.* **72** 3670–3
- [13] Chapman B E *et al* 2002 *Phys. Plasmas* **9** 2061–8
- [14] Franz P, Marrelli L, Piovesan P, Chapman B E, Martin P, Predebon I, Spizzo G, White R B and Xiao C 2004 *Phys. Rev. Lett.* **92** 125001
- [15] O'Connell R *et al* 2003 *Phys. Rev. Lett.* **91** 045002
- [16] Den Hartog D J *et al* 2006 *Rev. Sci. Instrum.* **77** 10F122
- [17] Craig D, Den Hartog D J, Ennis D A, Gangadhara S and Holly D 2007 *Rev. Sci. Instrum.* **78** 013103
- [18] Gangadhara S, Craig D, Ennis D A and Den Hartog D J 2006 *Rev. Sci. Instrum.* **77** 10F109
- [19] Chapman B E *et al* 2010 *Plasma Phys. Control. Fusion* **52** 124048
- [20] Roberts D E 1981 *J. Quant. Spectrosc. Radiat. Transfer* **26** 259–72
- [21] Ochando M A, Medina F, Zurro B, McCarthy K J, Pedrosa M A, Baciero A, Rapisarda D, Carmona J M and Jimnez D 2006 *Plasma Phys. Control. Fusion* **48** 1573
- [22] Reusch J A, Borchardt M T, Den Hartog D J, Falkowski A F, Holly D J, O'Connell R and Stephens H D 2008 *Rev. Sci. Instrum.* **79** 10E733
- [23] Lorenzini R, Auriemma F, Canton A and Carraro L 2006 *Phys. Plasmas* **13** 112510
- [24] Clayton D J, Almagri A F, Burke D R, Forest C B, Goetz J A, Kaufman M C and O'Connell R 2010 *Rev. Sci. Instrum.* **81** 10E308